Segmented Real-time Dispatch Model and Stochastic Robust Optimization for Power-gas Integrated Systems with Wind Power Uncertainty

Ying Wang, Kaiping Qu, and Kaifeng Zhang

***Abstract*—This paper develops a segmented real-time dispatch model for power-gas integrated systems (PGISs), where power-to-gas (P2G) devices and traditional automatic generation control units are cooperated to manage wind power uncertainty. To improve the economics of the real-time dispatch in regard to the current high operation cost of P2Gs, the wind power uncertainty set is divided into several segments, and a segmented linear decision rule is developed, which assigns adjustment tasks differently when wind power uncertainty falls into different segments. Thus, the P2G operation with high costs can be reduced in real-time adjustment. Besides, a novel segmented stochastic robust optimization is proposed to improve the efficiency and robustness of PGIS dispatch under wind power uncertainty, which minimizes the expected cost under the empirical wind power distribution and builds up the security constraints based on the robust optimization. The expected cost is formulated using a Nataf conversion-based multi-point estimate method, and the optimal number of estimate points is determined through sensitivity analysis. Furthermore, a difference-of-convex optimization with a partial relaxation rule is developed to solve the non-convex dispatch problem in a sequential optimization framework. Numerical simulations in two testing cases validate the effectiveness of the proposed model and solving method.**

***Index Terms*—Power-gas integrated system, robust optimization, real-time dispatch, multi-point estimate method, difference-of-convex optimization.**

NOMENCLATURE

A. Indices and Sets

Ξ_t	Wind uncertainty set
$\Xi_{t,s}$	Wind uncertainty subset s
Ω_{gc}	Set of coal-fired generation units
$\Omega_{\mathrm{cp}}, \Omega_{\mathrm{ncp}}$	Pipeline with and without a compressor
h	Index of gas sources
i	Index of automatic generation control (AGC) units
j	Index of power-to-gas (P2G) devices
k	Index of wind farms
s	Index of uncertainty subsets
t	Index of dispatch periods
v	Index of iteration steps in convexification of nonlinear constraints
w	Index of estimate points

B. Parameters and Functions

$\boldsymbol{\alpha}_{t,s}$	Participation factors
$[\underline{\pi}_t, \overline{\pi}_t]$	Forecasted lower and upper bounds of total uncertain wind power
$[\underline{\theta}, \overline{\theta}_t]$	Normalized lower and upper bounds of total uncertain wind power
σ_{mn}	Consumed gas flow of compressor mn
$\eta_i^{\mathrm{gt}}, \eta_j^{\mathrm{p2g}}$	Conversion efficiencies of gas turbine and P2G device
$\rho_{i,t}, \rho_{j,t}$	Adjustment cost coefficients of AGC unit i and P2G j
ρ_{w}	Penalty factor of wind curtailment
ρ	Penalty factor of relax variables
ω_w	Weight of the w^{th} estimate point
$\boldsymbol{\Phi}$	Cumulative distribution function (CDF) of the standard Gaussian distribution
a, b	Positive constants of convexification of nonlinear constraints
$\boldsymbol{A}_t, \boldsymbol{G}_t$	Constant matrices of security constraints of power system
$C(\cdot)$	Convex function associated with decision variables
$C_{i,t,s}$	Bilinear function concerning $\alpha_{i,t,s}$, $\tilde{\underline{\pi}}_t^{\mathrm{p2g}}$, and $\tilde{\overline{\pi}}_t^{\mathrm{agc}}$
c_{mn}	Gas flow transmission coefficient of pipe mn
$Cost(\cdot)$	Quadratic function of generation costs

Manuscript received: December 30, 2022; revised: March 6, 2023; accepted: April 24, 2023. Date of CrossCheck: April 24, 2023. Date of online publication: July 3, 2023.

This research was supported by the National Natural Science Foundation of China (No. 51907025) and Fundamental Research Funds for the Central Universities.

Y. Wang (corresponding author) and K. Zhang are with Key Laboratory of Measurement and Control of CSE, Ministry of Education, School of Automation, Southeast University, Nanjing, China (e-mail: wyseu@seu.edu.cn; kaifengzhang@seu.edu.cn).

K. Qu is with School of Electrical Engineering, China University of Mining and Technology, Xuzhou, China (e-mail: qukaiping@cumt.edu.cn).

DOI: 10.35833/MPCE.2022.000856

$\boldsymbol{c}_t$, $\boldsymbol{d}_t$ Constant vectors of security constraints of power system

$D_{j,t,s}$ Bilinear function concerning $\beta_{j,t,s}$, $\underline{\tilde{\pi}}_t^{\mathrm{p2g}}$, and $\overline{\tilde{\pi}}_t^{\mathrm{agc}}$

$\boldsymbol{e}$ Column vector whose cell values are 1

E_{g} Calorific value of natural gas

$\mathbb{E}_{p\in}$ Expected adjustment cost under empirical distribution

F_t^{-1} Inverse of CDF of total available wind power fluctuation

$g_{l,i}, g_{l,m}, g_{l,k}, g_{l,j}, g_{l,n}$ Shift factors of AGC unit i, non-AGC unit m, wind farm k, P2G device j, and load n to line l

$\boldsymbol{H}_t(\cdot)$ Bilinear function of decision variables $\boldsymbol{x}_t$

$\underline{K}_{mn}, \overline{K}_{mn}$ The minimum and maximum pressurizations of compressor mn

M_{req} Required line pack in gas network after dispatch

N Number of estimate points

P Empirical distribution

$P_{k,t}^{\mathrm{w,e}}$ Forecast expectation of wind farm k

$\underline{P}_i^{\mathrm{agc}}, \overline{P}_i^{\mathrm{agc}}$ The minimum and maximum power outputs of AGC unit i

$\underline{P}_m^{\mathrm{nagc}}, \overline{P}_m^{\mathrm{nagc}}$ The minimum and maximum power outputs of non-AGC unit m

$\overline{P}_j^{\mathrm{p2g}}$ The maximum power input of P2G j

$P_{n,t}^{\mathrm{d}}$ Power demand at node n in power network

$\underline{p}_n, \overline{p}_n$ The minimum and maximum gas pressures of node n in gas network

p_h Gas purchase price of gas source h

p_j Operation cost coefficient of P2G j

$\underline{q}_h^{\mathrm{s}}, \overline{q}_h^{\mathrm{s}}$ The minimum and maximum gas flow outputs of gas source h

$q_{n,t}^{\mathrm{d}}$ Gas demand of node n

r_m^-, r_m^+ The maximum ramp down and ramp up of non-AGC unit m

r_{mn} Line pack coefficient of pipe mn

$\underline{T}_l, \overline{T}_l$ The minimum and maximum limits of power line l

$[\underline{u}_{k,t}, \overline{u}_{k,t}]$ Forecasted lower and upper bounds of uncertain wind power fluctuation of wind farm k

$W(\cdot)$ Quadratic penalty function for wind curtailment

z_w The w^{th} estimate point of standard Gaussian distribution

C. Decision Variables

$\alpha_{i,t}^-, \alpha_{i,t}^+$ Participation factors of AGC unit i for downward and upward wind power fluctuations

$\beta_{j,t}^-, \beta_{j,t}^+$ Participation factors of P2G j for downward and upward wind power fluctuations

$\underline{\tilde{\pi}}_t^{\mathrm{p2g}}$ Allowable downward wind power fluctuation undertaken by P2Gs

$\overline{\tilde{\pi}}_t^{\mathrm{agc}}$ Allowable upward wind power fluctuation undertaken by traditional AGC units

$\overline{\tilde{\pi}}_t$ Total allowable upward wind power fluctuation

$\xi_{t,s}$ Endpoints of wind uncertainty subsets

δ_i Relax variable to convexify DC constraints

$\underline{\boldsymbol{\lambda}}_{t,s}, \overline{\boldsymbol{\lambda}}_{t,s}, \underline{\boldsymbol{\tau}}_{t,s}, \overline{\boldsymbol{\tau}}_{t,s}$ Dual variables of corresponding boundary constraints

$L_{l,t}$ Power flow of line l at time t

$M_{mn,t}$ Line pack in pipe mn

$P_{k,t}^{\mathrm{w}}$ Baseline power output of wind farm k

$P_{i,t}^{\mathrm{agc}}$ Baseline power output of AGC unit i

$P_{j,t}^{\mathrm{p2g}}$ Baseline power input of P2G j

$P_{m,t}^{\mathrm{nagc}}$ Baseline power output of non-AGC unit m

$p_{n,t}$ Gas pressure of node n in gas network

Q Adjustment cost in the second stage

$q_{h,t}^{\mathrm{s}}$ Baseline gas flow output of gas source h

$q_{mn,t}^{\mathrm{in}}, q_{mn,t}^{\mathrm{out}}$ Gas inflow and outflow of pipe mn

$q_{mn,t}$ Average gas flow of pipe mn

$\underline{\tilde{q}}_{i,t}^{\mathrm{gt}}, \overline{\tilde{q}}_{i,t}^{\mathrm{gt}}$ The minimum and maximum gas flow consumptions of gas turbine i

$\underline{\tilde{q}}_{j,t}^{\mathrm{p2g}}, \overline{\tilde{q}}_{j,t}^{\mathrm{p2g}}$ The minimum and maximum gas flow outputs of P2G j

$\underline{R}_{i,t}, \overline{R}_{i,t}$ Reserve down and up provided by AGC unit i

$\underline{S}_{j,t}, \overline{S}_{j,t}$ Reserve down and up provided by P2G j

x_1, y_1, x_2, y_2 Decision variables of convexification of nonlinear constraints

D. Uncertain Variables

$\hat{\pi}_t$ Total available wind power fluctuation of all wind farms

π_t Total allowable power fluctuation of all wind farms

$\hat{P}_{k,t}^{\mathrm{w}}$ Available wind power of wind farm k

$\tilde{P}_{k,t}^{\mathrm{w}}$ Actual power output of wind farm k

$\tilde{P}_{i,t}^{\mathrm{agc}}$ Actual power output of AGC unit i

$\tilde{P}_{i,t}^{\mathrm{p2g}}$ Actual power input of P2G j

$\tilde{q}_{i,t}^{\mathrm{gt}}$ Actual gas flow consumption of gas turbine i

$\tilde{q}_{i,t}^{\mathrm{p2g}}$ Actual gas flow output of P2G j

$\hat{u}_{k,t}$ Available wind power fluctuation of wind farm k

$u_{t,k}$ Allowable power fluctuation of wind farm k

I. Introduction

POWER-GAS integrated system (PGIS) can utilize the electricity and natural gas energy synergistically and interactively, which improves the energy efficiency and operation flexibility of the total system [1]. Recently, with the emerging power-to-gas (P2G) technology [2], it becomes possible to co-optimize traditional units and P2G devices to maintain the energy balance and address uncertainty issues from the increasing penetration of the renewable power integration, e.g., wind power [3]. By dynamically converting ex-

cess power from the power system into natural gas, P2Gs can fast respond to the dispatch signals and participate in the real-time dispatch [4]-[6], which is typically undertaken by traditional automatic generation control (AGC) units. Therefore, there is an important need to find an appropriate way to coordinate P2Gs and traditional AGC units in the real-time dispatch to address the uncertainty problems.

Currently, massive studies have been conducted on PGIS operations with wind power uncertainty. From the perspective of optimization models, mainstream methods can be classified into scenario-based optimization (SO) [7], [8], interval-based optimization (IO) [9], classical robust optimization (CRO) [10]-[12], and distributionally robust optimization (DRO) [13]. To hedge the wind power uncertainty, the above methods usually model the problem as a two-stage problem, which optimizes the baseline power in the first stage and conducts the adjustments in the second stage. The adjustments are usually obtained through re-optimizations in unit commitment and economic dispatch, but they need to be immediate decisions provided by the AGC system in the real-time dispatch. To meet the timeliness requirements of the real-time dispatch, linear decision-based optimization methods have been proposed, in which the baseline power is determined in the first-stage optimization and the adjustments are implemented through participation factors [14]. Participation factors, also called allocation coefficients or distribution factors, determine how much the AGC resources will undertake the adjustment task to level off the wind power fluctuations[14]. When the wind power deviates from its baseline power, the AGC resources, including the traditional AGC units and P2Gs, will adjust their outputs to compensate and smooth the wind power fluctuations. Accordingly, the above IO, CRO, and DRO methods need to be modified into linear decision-based IO [15], CRO [16], [17], and DRO methods [18]-[20] in the real-time dispatch.

Besides the problem regarding the optimization methods to deal with the uncertainty problems, another critical issue is how to coordinate P2Gs with traditional units in the PGIS. In day-ahead scheduling, the P2Gs are often optimized together with other resources [11]. In real-time dispatch, the participation factors of all the resources are usually determined beforehand based on their cost efficiencies [14], [16]-[21]. In addition, the reliability and environmental objectives with P2G operation constraints have been studied in [22], [23].

While many publications have studied either the PGIS operation optimizations with wind power uncertainty or PGIS real-time dispatch, much less attention has been directed to coordinating P2Gs and traditional AGC resources with wind power uncertainty in the real-time dispatch. Specifically, in the existing real-time dispatch models [14], [16]-[21], all the AGC resources usually follow the traditional linear decision rule with the participation factors that are already determined through optimization. In another sentence, the adjustment task will be assigned to these resources based on the fixed participation factors regardless of the real-time degree of the wind power uncertainty. As we know, the efficiency of converting power to natural gas is comparatively lower (50%-60%) [16], and thus it is expensive to keep the P2G operation all over the time [2]. In fact, it is costly and unnecessary for P2Gs to always participate in leveling off the wind power fluctuations. When the wind power fluctuates slightly, it is entirely possible to reduce or even shut down the P2G operation to enhance economical efficiency. To this end, we are motivated to upgrade the traditional linear decision rule into a segmented linear decision rule, which divides the wind power uncertainty into different segments, and assigns the adjustment task to the AGC resources by different decision rules when wind power uncertainty falls into different segments. With the segmented rule, the AGC resources, including the P2Gs, will be given different priorities to fulfill the adjustment task to improve the economics.

Moreover, it is noticed that most of the existing real-time dispatch methods of PGIS are based on IO, CRO, and DRO methods. In order to combine the benefits of stochastic and robust optimizations, we introduce stochastic robust optimization (SRO) [21] to the real-time dispatch of PGIS. The SRO method optimizes the expected cost under the empirical distribution and builds the security constraints with robust optimization. Considering that the empirical distribution better fits the wind power historical data and is closer to its actual distributions, the SRO tends to be more economical than traditional robust strategies under general wind distributions. Different from SRO, this work improves the SRO with a segmented linear decision rule to better coordinate the P2Gs and traditional AGC resources to increase the cost efficiencies. Meanwhile, compared with the SRO that only focuses on power system operation and formulates the empirical distribution with a three-point estimate method, this paper applies SRO to the PGIS and extends it to a multi-point estimate method, and the optimal number of the estimate points is determined by sensitivity analysis.

In this paper, we propose a segmented stochastic robust optimization (SSRO) method to better coordinate P2Gs and traditional AGC resources in the real-time dispatch of PGIS. The segmented linear decision rule actually upgrades parameterized wind uncertainty set into a variable-involved segmented uncertainty set. However, such a modification will make the security constraints in the power system non-convex and the gas flow transmission constraints are also intrinsically non-convex. To solve the real-time dispatch of PGIS with complex non-convex constraints, we design an effective convexified solution. To sum up, the main contributions of this paper are as follows.

1) A segmented real-time dispatch model of the PGIS is constructed to cooperate the traditional AGC units and P2Gs together to cope with the wind power uncertainty. With consideration of the high operation cost of P2Gs, a new segmented linear decision rule is proposed to assign the adjustment task differently when wind power uncertainty falls into different segments, leading to a lower total cost of the PGIS.

2) An SSRO is proposed to address the dispatch of PGIS under wind power uncertainty. With SSRO, the security constraints are built up with robust optimization to increase the system safety, while the expected cost under the empirical distribution is optimized based on stochastic optimization to

reach economical efficiency. A multi-point estimate method is developed for the expected cost formulation.

3) A partial relaxation-based difference-of-convex optimization (DCO) is developed to solve the non-convex dispatch problem. To be specific, the bilinear constraints converted from the uncertain constraints from the power system and the non-convex constraints from the gas system are equivalently transformed to difference-of-convex (DC) constraints with the tight and relaxed rule, respectively, and then solved by DCO method. Besides, a sequential optimization procedure is developed to correct the initialization of convexification.

II. Literature Review

A. PGIS Operation with Wind Power Uncertainty

As stated in the introduction, typical methods for optimizing the PGIS operation with wind power uncertainties include SO, IO, CRO, and DRO. The common thread of the SO, IO, CRO, and DRO methods is to minimize the operating cost with sufficient resources to accommodate real-time uncertainty, but they differ in uncertainty representations and mathematical formulations. In specific, [7] and [8] propose the scenario-based stochastic optimization method, which describes wind uncertainty with sampled scenarios and establishes security constraints in all scenarios. However, scenario-based methods can hardly cover all the extreme scenarios since the number of scenarios is restricted by the computation effort. Different from stochastic optimization, interval or robust methods guarantee the system safety under the worst case within an interval or uncertainty set. Existing robust optimization methods mainly include CRO and DRO. CRO describes the wind uncertainty by uncertainty set, i.e., the feasible region of wind power scenarios [11], [12]. CRO usually minimizes the cost in the worst-case scenarios or the expected scenario, which ignores the probability distributions of the wind power, and the optimization results generally tend to be conservative or inefficient [24]. As for DRO, it uses an ambiguous set to describe wind uncertainty, i.e., the feasible region of wind distributions. Commonly-used ambiguous set includes probability density-based [25], distance-based [26], [27], and statistical moments-based methods [28], [29]. DRO minimizes the expected cost under extreme wind distributions, which is less conservative than CRO.

To combine the advantages of the above-mentioned methods, some hybrid optimization methods, e.g., stochastic interval optimization (SIO) [30]-[32] and SRO [33], [34] methods, are proposed. In [30], the SO and IO are implemented sequentially over the horizon with a switching time to balance the cost and security premium in the power systems. In [31], [32], scenarios and uncertainty sets are used for modeling different uncertain variables in multi-energy systems. Reference [33] proposes an SRO for power system unit commitment, which considers both the scenario-based expected cost and the worst-case cost in the objective function. The SRO in [34] models the wind power and price uncertainties by uncertainty set and scenarios, respectively. However, the above methods can hardly be directly applied to real-time dispatch due to the timeliness requirements in real-time dispatch.

B. Real-time Dispatch with Wind Uncertainty

To meet the timeliness requirement of real-time dispatch, linear decision-based optimization methods are proposed, in which the baseline power and the participation factors are determined. References [16] and [17] establish the optimal dispatch for the PGIS with the linear decision-based CRO method. However, these methods usually optimize the baseline operation cost but ignore the adjustment cost. Compared with the linear decision-based CRO, the linear decision-based DRO takes the baseline cost and the adjustment cost into account by minimizing the expected cost under the extreme distributions, and thus the linear decision-based DRO is generally superior to the linear decision-based CRO in term of cost efficiency. However, the linear decision-based DRO focuses only on the expected cost under extreme distributions while ignoring the expected cost under general distributions, and thus it is less economical under most possible distributions because the extreme distributions rarely occur. In order to improve the economy of linear decision-based robust optimization under general distributions, [21] proposes the linear decision-based SRO for power system dispatch problems, which formulates the expected generation cost under the empirical wind distribution in the objective and satisfies the system security constraints within the uncertainty set. However, the above literature has not specifically considered how to coordinate P2Gs and traditional AGC units in setting the participation factors.

III. Segmented Real-time Dispatch

A. General Idea of Segmented Real-time Dispatch

To cope with the wind power uncertainty, real-time dispatch optimizes the baseline state of generation units, wind power and gas sources as well as the participation factors of AGC resources. When wind power deviates from the baseline state, AGC resources regulate to neutralize the power imbalance, while non-AGC resources will operate at the baseline state. In general, when wind power fluctuates upward, the generation-side AGC units need to decrease the output power while the load-side AGC resources need to increase the power consumption. In contrast, when wind power fluctuates downward, the generation-side AGC units need to increase the output power while the load-side AGC resources need to decrease the power consumption.

In this paper, the AGC resources mainly include the AGC units and P2Gs. With regard to the current inadequate conversion efficiency and high cost of P2Gs (water electrolysis and methanation) [2], [16], the PGIS will tend to make less use of the P2Gs in the real-time adjustment. Therefore, we propose a segmented real-time dispatch model for the PGIS, which sets different dispatch strategies of the AGC units and the P2Gs when the wind power uncertainty falls into different segments. The general idea of the segmented real-time dispatch at different uncertainty levels is illustrated in Fig. 1. The wind power uncertainty, i.e., the forecast error, is divid-

ed into four segments. When the wind power uncertainty fluctuates upward and falls into segment ②, all the adjustment tasks will be assigned to the traditional AGC units, and the P2G devices will be kept at the baseline power. When the wind power uncertainty exceeds the adjustment capability of the traditional AGC units and falls into segment ①, the traditional AGC units will decrease the output at first until reaching their maximum adjustment capability, and then P2G devices will increase the power consumption to fulfill the remaining adjustment task. Similarly, when wind power fluctuates downward, the wind power uncertainty may fall into segments ③ and ④. In these two segments, the P2Gs are given priority to decrease the power input due to their high costs. When the wind power uncertainty exceeds the P2G adjustment capability, the exceeding part will be assigned to the traditional AGC units.

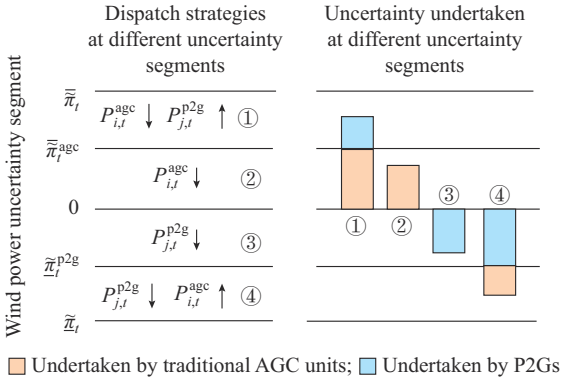

Fig. 1. Illustration of segmented real-time dispatch at different uncertainty levels.

B. Wind Power Uncertainty Set

For each wind farm, $\hat{P}^{\mathrm{w}}_{k,t}$ is represented as the summation of $P^{\mathrm{w,e}}_{k,t}$ and $\hat{u}_{k,t}$, i.e.,

$$\hat{P}^{\mathrm{w}}_{k,t}=P^{\mathrm{w,e}}_{k,t}+\hat{u}_{k,t} \tag{1}$$

$\hat{u}_{k,t}$ and $\hat{\pi}_t$ are assumed to be in the forecast intervals:

$$\underline{u}_{k,t}\le\hat{u}_{k,t}\le\bar{u}_{k,t} \tag{2}$$

$$\underline{\pi}_t\le\hat{\pi}_t\le\bar{\pi}_t \quad \hat{\pi}_t=\sum_k\hat{u}_{k,t} \tag{3}$$

In the real-time dispatch, the forecasted available wind power within $[\underline{\pi}_t,\bar{\pi}_t]$ cannot be fully integrated into the PGIS when it exceeds its adjustment capability, and then the excessive power will be curtailed. The wind power curtailment strategy can be described as:

$$\tilde{P}^{\mathrm{w}}_{k,t}=\begin{cases}P^{\mathrm{w}}_{k,t}+\hat{u}_{k,t} & \hat{\pi}_t\le\bar{\tilde{\pi}}_t\\ P^{\mathrm{w}}_{k,t}+\underline{u}_{k,t}+\dfrac{\bar{\tilde{\pi}}_t-\underline{\pi}_t}{\hat{\pi}_t-\underline{\pi}_t}(\hat{u}_{k,t}-\underline{u}_{k,t}) & \hat{\pi}_t>\bar{\tilde{\pi}}_t\end{cases} \tag{4}$$

$\bar{\tilde{\pi}}_t$ is smaller than the forecast upper bound:

$$\bar{\tilde{\pi}}_t\le\bar{\pi}_t \tag{5}$$

When taking the the allowable upward wind power fluctuation into consideration, the uncertainty set of the allowable wind power can be described as:

$$\Xi_t=\left\{\boldsymbol{u}_t\middle|\underline{u}_{k,t}\le u_{k,t}\le\bar{u}_{k,t};\ \underline{\pi}_t\le\pi_t\le\bar{\tilde{\pi}}_t;\ \sum_k u_{k,t}=\pi_t\right\} \tag{6}$$

C. Segmented Linear Decision Rule-based Real-time Dispatch

In the dispatch mode, the traditional linear decision rule is upgraded to the segmented linear decision rule. The wind power uncertainty, i.e., the total wind power fluctuation, is first divided into four segments.

$$\Xi_t=\left\{\boldsymbol{u}_t\middle|\underline{u}_{k,t}\le u_{k,t}\le\bar{u}_{k,t};\xi_{t,s-1}\le\sum_k u_{k,t}\le\xi_{t,s}\right\}\quad\forall s\le 4 \tag{7}$$

where $\xi_{t,0}=\underline{\pi}_t$, $\xi_{t,1}=\underline{\tilde{\pi}}^{\mathrm{p2g}}_t$, $\xi_{t,2}=0$, $\xi_{t,3}=\bar{\tilde{\pi}}^{\mathrm{agc}}_t$, $\xi_{t,4}=\bar{\tilde{\pi}}_t$, and they satisfy:

$$\xi_{t,s-1}\le\xi_{t,s}\quad\forall s \tag{8}$$

The adjustment task is assigned to resources by different decision rules when wind power uncertainty falls into different segments.

1) When the wind power uncertainty falls into segment ② in Fig. 1, i.e., wind power fluctuates little upward and does not exceed the maximum adjustment capability of the AGC units, AGC units will reduce the power output, and the P2Gs will stay at the baseline power as:

$$\begin{cases}\tilde{P}^{\mathrm{agc}}_{i,t}=P^{\mathrm{agc}}_{i,t}-\alpha^{+}_{i,t}\pi_t\\ \tilde{P}^{\mathrm{p2g}}_{j,t}=P^{\mathrm{p2g}}_{j,t}\end{cases}\quad\pi_t\in[0,\bar{\tilde{\pi}}^{\mathrm{agc}}_t] \tag{9}$$

2) When the wind power uncertainty falls into segment ① in Fig. 1, i.e., wind power fluctuates upward and exceeds the maximum adjustment capability of the AGC units, AGC units will reduce the power output until reaching the maximum adjustment capability and the P2Gs increase the power consumption to fulfill the remaining part as:

$$\begin{cases}\tilde{P}^{\mathrm{agc}}_{i,t}=P^{\mathrm{agc}}_{i,t}-\alpha^{+}_{i,t}\bar{\tilde{\pi}}^{\mathrm{agc}}_t\\ \tilde{P}^{\mathrm{p2g}}_{j,t}=P^{\mathrm{p2g}}_{j,t}+\beta^{+}_{j,t}(\pi_t-\bar{\tilde{\pi}}^{\mathrm{agc}}_t)\end{cases}\quad\pi_t\in[\bar{\tilde{\pi}}^{\mathrm{agc}}_t,\bar{\tilde{\pi}}_t] \tag{10}$$

3) When the wind power uncertainty falls into segment ③ in Fig. 1, i.e., wind power fluctuates downward and does not exceed the maximum adjustment capability of the P2Gs, P2Gs will reduce the power consumption as:

$$\begin{cases}\tilde{P}^{\mathrm{agc}}_{i,t}=P^{\mathrm{agc}}_{i,t}\\ \tilde{P}^{\mathrm{p2g}}_{j,t}=P^{\mathrm{p2g}}_{j,t}+\beta^{-}_{j,t}\pi_t\end{cases}\quad\pi_t\in[\underline{\tilde{\pi}}^{\mathrm{p2g}}_t,0] \tag{11}$$

4) When the wind power uncertainty falls into segment ④ in Fig. 1, i.e., wind power fluctuates downward and exceeds the maximum adjustment capability of the traditional P2Gs, P2Gs will reduce the power consumption until reaching the maximum adjustment capability and the AGC units increase the power output to fulfill the remaining part as:

$$\begin{cases}\tilde{P}^{\mathrm{agc}}_{i,t}=P^{\mathrm{agc}}_{i,t}-\alpha^{-}_{i,t}(\pi_t-\underline{\tilde{\pi}}^{\mathrm{p2g}}_t)\\ \tilde{P}^{\mathrm{p2g}}_{j,t}=P^{\mathrm{p2g}}_{j,t}+\beta^{-}_{j,t}\underline{\tilde{\pi}}^{\mathrm{p2g}}_t\end{cases}\quad\pi_t\in[\underline{\pi}_t,\underline{\tilde{\pi}}^{\mathrm{p2g}}_t] \tag{12}$$

In the above four situations, constraints (13) and (14) need to be satisfied.

$$\begin{cases} \alpha_{i,t}^{+} \geq 0 \\ \alpha_{i,t}^{-} \geq 0 \\ \sum_i \alpha_{i,t}^{+} = 1 \\ \sum_i \alpha_{i,t}^{-} = 1 \end{cases} \tag{13}$$

$$\begin{cases} \beta_{j,t}^{+} \geq 0 \\ \beta_{j,t}^{-} \geq 0 \\ \sum_j \beta_{j,t}^{+} = 1 \\ \sum_j \beta_{j,t}^{-} = 1 \end{cases} \tag{14}$$

The above segmented decision rule can be described in a compact form as

$$\begin{cases} \tilde{P}_{i,t}^{\text{agc}} = P_{i,t}^{\text{agc}} - \alpha_{i,t,s} \sum_k u_{k,t} + C_{i,t,s} \\ \tilde{P}_{j,t}^{\text{p2g}} = P_{j,t}^{\text{p2g}} + \beta_{j,t,s} \sum_k u_{k,t} + D_{j,t,s} \end{cases} \quad \forall s \tag{15}$$

D. Constraints

The constraints of the PGIS mainly include the power system constraints [35], the natural gas system constraints [36], and the coupling constraints.

1) Security Constraints of Power System

In the following context, x and $\tilde{x}$ represent the baseline and the actual value of the decision variables, respectively; $\underline{\tilde{x}}$ and $\overline{\tilde{x}}$ represent the possible extreme boundaries at the adjustment stage; and $\underline{x}$ and $\bar{x}$ represent the actual minimum and maximum limits, respectively.

$$\sum_i P_{i,t}^{\text{agc}} + \sum_m P_{m,t}^{\text{nagc}} + \sum_k P_{k,t}^{\text{w}} - \sum_j P_{j,t}^{\text{p2g}} - \sum_n P_{n,t}^{\text{d}} = 0 \tag{16}$$

$$-\underline{u}_{k,t} \leq P_{k,t}^{\text{w}} \leq P_{k,t}^{\text{w,e}} \quad \forall k \tag{17}$$

$$\begin{cases} -\alpha_{i,t}^{+} \overline{\tilde{\pi}}_t^{\text{agc}} \geq \underline{R}_{i,t} \\ -\alpha_{i,t}^{-} (\underline{\pi}_t - \underline{\tilde{\pi}}_t^{\text{p2g}}) \leq \overline{R}_{i,t} \end{cases} \quad \forall i \tag{18}$$

$$\begin{cases} \underline{P}_i^{\text{agc}} \leq P_{i,t}^{\text{agc}} + \underline{R}_{i,t} \\ P_{i,t}^{\text{agc}} + \overline{R}_{i,t} \leq \overline{P}_i^{\text{agc}} \end{cases} \quad \forall i \tag{19}$$

$$P_{i,t}^{\text{agc}} + \underline{R}_{i,t} - (P_{i,t-1}^{\text{agc}} + \overline{R}_{i,t-1}) \geq -r_i^{-} \quad \forall i \tag{20}$$

$$P_{i,t}^{\text{agc}} + \overline{R}_{i,t} - (P_{i,t-1}^{\text{agc}} + \underline{R}_{i,t-1}) \leq r_i^{+} \quad \forall i \tag{21}$$

$$\begin{cases} \beta_{j,t}^{-} \tilde{\pi}_t^{\text{p2g}} \geq \underline{S}_{j,t} \\ \beta_{j,t}^{+} (\overline{\tilde{\pi}}_t - \overline{\tilde{\pi}}_t^{\text{agc}}) \leq \overline{S}_{j,t} \end{cases} \quad \forall j \tag{22}$$

$$\begin{cases} 0 \leq P_{j,t}^{\text{p2g}} + \underline{S}_{j,t} \\ P_{j,t}^{\text{p2g}} + \overline{S}_{j,t} \leq \overline{P}_j^{\text{p2g}} \end{cases} \quad \forall j \tag{23}$$

$$\underline{P}_m^{\text{nagc}} \leq P_{m,t}^{\text{nagc}} \leq \overline{P}_m^{\text{nagc}} \quad \forall m \tag{24}$$

$$-r_m^{-} \leq P_{m,t}^{\text{nagc}} - P_{m,t-1}^{\text{nagc}} \leq r_m^{+} \quad \forall m \tag{25}$$

Formula (16) represents the power balance constraint of the power system; (17) represents the minimum and maximum limits of the baseline wind power; (18) and (19) represent the minimum and maximum power limits of the AGC units, respectively; (20) and (21) represent the ramping limits of the AGC units; (22) and (23) represent the minimum and maximum power input limits of the P2Gs, respectively; and (24) and (25) represent the power limits and ramping limits of the non-AGC units, respectively.

Note that the extreme adjustment of AGC units and P2Gs is caused by extreme total wind power fluctuations. Therefore, power output/input limits of AGC units and P2Gs are established by extreme scenarios, as shown in (18) and (22). However, the power flow in transmission lines depends on the actual power output of each wind farm and cannot be described by extreme scenarios. To address this problem, the uncertain variable $\boldsymbol{u}_t$ is introduced into the power flow constraints as:

$$\begin{cases} \underline{T}_l \leq -\sum_i g_{l,i} \left(\alpha_{i,t,s} \sum_k u_{k,t} - C_{i,t,s} \right) - \sum_j g_{l,j} \left(\beta_{j,t,s} \sum_k u_{k,t} + D_{j,t,s} \right) + L_{l,t} + \sum_k g_{l,k} u_{k,t} \leq \overline{T}_l \quad \forall \boldsymbol{u}_t \in \Xi_{t,s} \\ L_{l,t} = \sum_i g_{l,i} P_{i,t}^{\text{agc}} + \sum_m g_{l,m} P_{m,t}^{\text{nagc}} + \sum_k g_{l,k} P_{k,t}^{\text{w}} - \sum_j g_{l,j} P_{j,t}^{\text{p2g}} - \sum_n g_{l,n} P_{n,t}^{\text{d}} \end{cases} \tag{26}$$

To sum up, the security constraints of the power system can be described in the following unified form.

$$\boldsymbol{A}_t \boldsymbol{x}_t + \boldsymbol{\alpha}_{t,s} \boldsymbol{x}_t \leq \boldsymbol{c}_t \quad \forall t, s \tag{27}$$

$$\boldsymbol{H}_t(\boldsymbol{x}_t) + \max_{\boldsymbol{u}_t \in \Xi_{t,s}} (\boldsymbol{G}_t \boldsymbol{\alpha}_{t,s} \boldsymbol{u}_t) \leq \boldsymbol{d}_t \quad \forall t, s \tag{28}$$

Note that (28) contains the uncertain variables, and it can be transferred into the deterministic constraints using dual theory as:

$$\begin{cases} \boldsymbol{H}_t(\boldsymbol{x}_t) + \overline{\boldsymbol{\lambda}}_{t,s} \overline{\boldsymbol{u}}_t - \underline{\boldsymbol{\lambda}}_{t,s} \underline{\boldsymbol{u}}_t + \overline{\boldsymbol{\tau}}_{t,s} \xi_{t,s} - \underline{\boldsymbol{\tau}}_{t,s} \xi_{t,s-1} \leq \boldsymbol{d}_t \\ -\boldsymbol{G}_t \boldsymbol{\alpha}_{t,s} + \overline{\boldsymbol{\lambda}}_{t,s} - \underline{\boldsymbol{\lambda}}_{t,s} + \overline{\boldsymbol{\tau}}_{t,s} \boldsymbol{e}^{\text{T}} - \underline{\boldsymbol{\tau}}_{t,s} \boldsymbol{e}^{\text{T}} = \boldsymbol{0} \end{cases} \tag{29}$$

2) Security Constraints of Natural Gas System

In the natural gas system, natural gas loads are supplied by natural gas sources through pipelines and compressor stations [36]. The gas flow constraints include (30)-(39).

$$\sum_{h \in n} q_{h,t}^{\text{s}} + \sum_{j \in n} \tilde{q}_{j,t}^{\text{p2g}} - \sum_{i \in n} \tilde{q}_{i,t}^{\text{gt}} - q_{n,t}^{\text{d}} + \sum_{m \in U(n)} q_{mn,t}^{\text{out}} - \sum_{m' \in D(n)} q_{nm',t}^{\text{in}} = 0 \quad \forall n \tag{30}$$

$$\underline{q}_h^{\text{s}} \leq q_{h,t}^{\text{s}} \leq \overline{q}_h^{\text{s}} \quad \forall h \tag{31}$$

$$\underline{p}_n \leq p_{n,t} \leq \overline{p}_n \quad \forall n \tag{32}$$

$$M_{mn,t} = M_{mn,t-1} + (q_{mn,t}^{\text{in}} - q_{mn,t}^{\text{out}}) \Delta t \quad \forall mn \in \Omega_{\text{ncp}} \tag{33}$$

$$M_{mn}^{t} = r_{mn} (p_{m,t} + p_{n,t})/2 \quad \forall mn \in \Omega_{\text{ncp}} \tag{34}$$

$$\sum_{mn \in \Omega_{\text{ncp}}} M_{mn,T} \geq M_{\text{req}} \tag{35}$$

$$q_{mn,t}^{2} = c_{mn} (p_{m,t}^{2} - p_{n,t}^{2}) \quad \forall mn \in \Omega_{\text{ncp}} \tag{36}$$

$$q_{mn,t}=(q_{mn,t}^{\text{in}}+q_{mn,t}^{\text{out}})/2 \quad \forall mn\in\Omega_{\text{ncp}} \tag{37}$$

$$\underline{K}_{mn}p_{m,t}\le p_{n,t}\le \overline{K}_{mn}p_{m,t} \quad \forall mn\in\Omega_{\text{cp}} \tag{38}$$

$$q_{mn,t}^{\text{out}}=(1-\sigma_{mn})q_{mn,t}^{\text{in}} \quad \forall mn\in\Omega_{\text{cp}} \tag{39}$$

Formula (30) represents the gas flow balance constraint of the natural gas system; (31) represents the output limit of the gas source; (32) represents the nodal gas pressure limit; (33)-(35) represent the line pack constraints of the pipeline without a compressor; (34) indicates the line pack stored in the pipeline *mn* is proportional to the average gas pressure of the pipeline; (35) indicates that the total line pack stored in the natural gas system cannot be lower than a specified value M_{req} after dispatch; (36) and (37) indicate that the average gas flow in the pipeline is related to the gas pressures of the two ends; (38) and (39) represent the constraints of the pipeline with the compressor; (38) represents the pressurization ratio limits of the compressor; and (39) represents the gas consumption of the compressor.

For the P2Gs and natural gas turbines which participate in the AGC service, they need to respond to the uncertain wind power, and further bring the uncertainty and fluctuations to the gas output (P2Gs) or input (gas turbine) of the natural gas system. In practice, the above gas uncertainty will be mainly balanced by the line pack in the pipeline, which leads to pressure fluctuations in the pipeline. Extreme fluctuations of the gas pressure will possibly bring about low-pressure or high-pressure events [17]. Therefore, the security constraints of the natural gas system in the extreme scenarios caused by gas turbines and P2Gs are considered. The security constraints under three extreme scenarios are formulated as (40), in which the equivalent gas inputs/outputs of the gas turbines and P2Gs are the minimum, maximum, and baseline values, respectively.

$$\begin{cases} \tilde{\underline{q}}_{h,t}^{\text{s}}=\tilde{\overline{q}}_{h,t}^{\text{s}}=q_{h,t}^{\text{s}} \quad \forall h \\ G\left(\underline{\tilde{\boldsymbol{x}}}\,\middle|\,\tilde{q}_{i,t}^{\text{gt}}=\tilde{\underline{q}}_{i,t}^{\text{gt}},\tilde{q}_{j,t}^{\text{p2g}}=\tilde{\overline{q}}_{j,t}^{\text{p2g}}\right) \\ G\left(\tilde{\overline{\boldsymbol{x}}}\,\middle|\,\tilde{q}_{i,t}^{\text{gt}}=\tilde{\overline{q}}_{i,t}^{\text{gt}},\tilde{q}_{j,t}^{\text{p2g}}=\tilde{\underline{q}}_{j,t}^{\text{p2g}}\right) \\ G\left(\boldsymbol{x}\,\middle|\,\tilde{q}_{i,t}^{\text{gt}}=q_{i,t}^{\text{gt}},\tilde{q}_{j,t}^{\text{p2g}}=q_{j,t}^{\text{p2g}}\right) \end{cases} \tag{40}$$

3) Coupling Constraints

The power system and natural gas system are coupled through the gas turbines and P2Gs, and the coupling constraint are given as:

$$\begin{cases} \tilde{\underline{q}}_{i,t}^{\text{gt}}=(P_{i,t}^{\text{gt}}+\underline{R}_{i,t})/(\eta_i^{\text{gt}}E_{\text{g}}) \\ \tilde{\overline{q}}_{i,t}^{\text{gt}}=(P_{i,t}^{\text{gt}}+\overline{R}_{i,t})/(\eta_i^{\text{gt}}E_{\text{g}}) \quad \forall i \\ q_{i,t}^{\text{gt}}=P_{i,t}^{\text{gt}}/(\eta_i^{\text{gt}}E_{\text{g}}) \end{cases} \tag{41}$$

$$\begin{cases} \tilde{\underline{q}}_{j,t}^{\text{p2g}}=\eta_j^{\text{p2g}}(P_{j,t}^{\text{p2g}}+\underline{S}_{j,t})/E_{\text{g}} \\ \tilde{\overline{q}}_{j,t}^{\text{p2g}}=\eta_j^{\text{p2g}}(P_{j,t}^{\text{p2g}}+\overline{S}_{j,t})/E_{\text{g}} \quad \forall j \\ q_{j,t}^{\text{p2g}}=\eta_j^{\text{p2g}}P_{j,t}^{\text{p2g}}/E_{\text{g}} \end{cases} \tag{42}$$

E. Objective Function

The segmented real-time dispatch model optimizes the baseline cost in the first stage and the expected adjustment cost in the second stage, as shown in (43). The baseline cost includes the fuel cost of generation units, the cost of gas sources, and the operation cost of P2Gs.

$$\min_x \left\{ \sum_t \sum_{i\in\Omega_{\text{gc}}} Cost_i(P_{i,t}^{\text{agc}}) + \sum_t \sum_{m\in\Omega_{\text{gc}}} Cost_m(P_{m,t}^{\text{nagc}}) + \sum_t \sum_h p_h q_{h,t}^{\text{s}} + \sum_t \sum_j p_j q_{j,t}^{\text{p2g}} + \mathbb{E}_{p\in}(Q(\boldsymbol{x},\hat{\boldsymbol{\pi}})) \right\} \tag{43}$$

Note that the operation cost of P2Gs is mainly associated with the cost of electric power and the cost of materials, i.e., H_2O in the water electrolysis and CO_2 in the methanation and other catalysts. The electric power cost of P2Gs has already been included in the generation cost of units, and hence the operation cost coefficient of P2Gs p_j actually indicates the material cost.

The generation costs of coal-fired generation units are quadratic functions associated with their outputs as:

$$\begin{cases} Cost_i(P_{i,t}^{\text{agc}})\ge a_i(P_{i,t}^{\text{agc}})^2+b_iP_{i,t}^{\text{agc}}+c_i \\ Cost_m(P_{m,t}^{\text{nagc}})\ge a_m(P_{m,t}^{\text{nagc}})^2+b_mP_{m,t}^{\text{nagc}}+c_m \end{cases} \tag{44}$$

Traditionally, the expected value is modeled by the random sampling method. However, the results of random samplings depend on the sampled points, and an accurate estimation usually requires sampling a large number of points. Thus, this paper conducts the multi-point estimate method, which is indeed a deterministic estimate method and can uniformly cover the uncertain wind power fluctuation with fewer estimate points [37]. Here, the uncertain variable in the multi-point estimate method is the total available wind power fluctuation. The wind power variables between different time periods are assumed to be independent of each other, and thus the multi-point estimate method is indeed to estimate the expected response function of a single uncertain variable as:

$$\mathbb{E}_{p\in}(Q(\boldsymbol{x},\hat{\boldsymbol{\pi}}))=\sum_t\sum_{w\in N}\omega_wQ_t(\boldsymbol{x}_t,\hat{\pi}_{t,w}) \tag{45}$$

$$\hat{\pi}_{t,w}=F_t^{-1}(\Phi(z_w)) \tag{46}$$

The number of estimate points ($N\ge 3$) is usually an odd number for reaching a certain accuracy [38]. The values of the estimate point z_w and the corresponding weights with different N are available in [38]. The sensitivity analysis of N will be conducted in the case studies. The adjustment cost in the second stage includes the adjustment costs of the AGC units and P2Gs, and the penalty costs of the wind power curtailment. For each estimate point of the total available wind power fluctuations ($\hat{\pi}_{t,w}$), we assume that when the estimate point is within the *s*th uncertainty segment, the corresponding sign variable $\sigma_{t,w,s}$ is 1, otherwise 0. The second-stage adjustment cost at each estimate point is given as:

$$\begin{cases} \pi_{t,w}\le\hat{\pi}_{t,w} \\ \pi_{t,w}\le\tilde{\overline{\pi}}_t \end{cases} \tag{47}$$

$$\begin{cases}\Delta\tilde{P}^{\text{agc}}_{i,t,w,s}\geq-\alpha_{i,t,s}\pi_{t,w}+C_{i,t,s}\\ \Delta\tilde{P}^{\text{p2g}}_{j,t,w,s}\leq\beta_{j,t,s}\pi_{t,w}+D_{j,t,s}\end{cases}\tag{48}$$

$$Q_t(\boldsymbol{x}_t,\hat{\pi}_{t,w})=\sum_s\sigma_{t,w,s}\left(\sum_i\rho_{i,t}\Delta\tilde{P}^{\text{agc}}_{i,t,w,s}+\sum_j\rho_{j,t}\Delta\tilde{P}^{\text{p2g}}_{j,t,w,s}\right)+\rho_{\text{w}}\left[\sum_k(P^{\text{w,e}}_{k,t}-P^{\text{w}}_{k,t})+\hat{\pi}_{t,w}-\pi_{t,w}\right]\tag{49}$$

IV. Solution Methodology

A. Convexification of Nonlinear Constraints

The nonlinear constraints in this model include the bilinear constraints (18), (22), (29) of the power system and the gas flow transmission constraint (36) of the natural gas system. This paper adopts DCO to deal with nonlinear constraints. One of the features of DCO is that the constraints of the optimization problem are convex or can be expressed as the difference between two convex functions. For example, xy can be expressed as $0.5[(x+y)^2-x^2-y^2]$. In view of this, the bilinear constraints (18), (22), (29) expressed in the compact form as (50) are transformed to DC constraint as (51).

$$\sum ax_1y_1-\sum bx_2y_2+C(x,y)\leq0\tag{50}$$

$$C(x,y)+\sum0.5a\left[(x_1+y_1)^2-x_1^2-y_1^2\right]+\sum0.5b\left[(x_2-y_2)^2-x_2^2-y_2^2\right]\leq0\tag{51}$$

Then, gas flow transmission constraint (36) is replaced by two inequations (51) and (52), where (51) is a second-order cone constraint (convex) and (52) is non-convex as a DC constraint.

$$q^2_{mn,t}/c_{mn}+p^2_{n,t}-p^2_{m,t}\leq0\tag{52}$$

$$p^2_{m,t}-p^2_{n,t}-q^2_{mn,t}/c_{mn}\leq0\tag{53}$$

Thus, the real-time dispatch of PGIS with nonlinear constraints is converted to the below compact form with DC constraints.

$$\begin{cases}\min F(x)\\ \text{s.t. } f_i(x)-g_i(x)\leq0\end{cases}\tag{54}$$

Furthermore, the DCO is introduced to optimize the problem (53). The problem is convexified as:

$$\begin{cases}\min\left(F_v(x)+\sum_i\rho_v\delta_i\right)\\ \text{s.t. } f_i(x)-[g_i(x_v)+(\nabla g_i(x_v))^{\text{T}}(x-x_v)]\leq\delta_i\\ \quad\delta_i\geq0\end{cases}\tag{55}$$

DCO iteratively updates the linearized base point and solves the updated problem to look for a high-quality solution. The algorithm converges when the optimization results of the two steps are close enough [39], [40]. Please see Algorithm 1 for the detailed steps of the DCO.

$$F_v-F_{v+1}\leq\varepsilon_1F_{v+1}\tag{56}$$

$$\max_i\delta_i\leq\varepsilon_2\tag{57}$$

Algorithm 1: DCO for the non-convex problem

Step 1: initialization: given an initial solution $\boldsymbol{x}_0$, let the iteration step $v=0$

Step 2: convexification: convexify the nonlinear constraint by (54), and solve the convex problem

Step 3: stop when the following conditions (56) and (57) hold or the maximum iteration step limit is reached; otherwise, update $\rho_{v+1}=\min(k_c\rho_v,\rho_{\max})$, $v=v+1$, and go to *Step 2*.

Partial relaxation rule: in this paper, a partial relaxation rule is incorporated into the DCO to accelerate the convergence of the algorithm. To be specific, it is found that the decision variables in nonlinear constraints in the power system ($\forall i\in P$) have large impacts on the objective function. As a result, it usually requires many iterations in DCO for the relaxed variables δ_i to converge to 0. Therefore, we let the relaxed variables in nonlinear power flow constraints to be strictly equal to 0, and these constraints hold strictly during the iteration process to speed up the convergence. As for the nonlinear gas flow constraints ($\forall i\in G$), the decision variables have minor impacts on the objective function, and meanwhile, it is difficult to find an initial feasible solution. Thus, there is no need to let the relaxed variable to be 0 for nonlinear gas flow constraints.

B. Initialization

For the nonlinear constraints in the power system ($\forall i\in P$), the initial point must be a feasible solution. Note that if the initial solution is feasible, the iteration will also be feasible for the convexification when letting the relaxed variable be 0 [38].

Firstly, the nonlinear constraints (18), (22), and (29) are linearized using the extreme scenarios as:

$$\begin{cases}\sum_i\underline{R}_{i,t}=-\overline{\tilde{\pi}}^{\text{agc}}_t\\ \sum_i\overline{R}_{i,t}=-(\underline{\pi}_t-\underline{\tilde{\pi}}^{\text{p2g}}_t)\end{cases}\tag{58}$$

$$\begin{cases}\sum_j\underline{S}_{j,t}=\underline{\tilde{\pi}}^{\text{p2g}}_t\\ \sum_j\overline{S}_{j,t}=(\overline{\tilde{\pi}}_t-\overline{\tilde{\pi}}^{\text{agc}}_t)\end{cases}\tag{59}$$

$$\begin{cases}\underline{\vartheta}_{l,k,t}\leq0\leq\overline{\vartheta}_{l,k,t}\\ \underline{\theta}_{l,t}\leq0\leq\overline{\theta}_{l,t}\\ \underline{\vartheta}_{l,k,t}\leq g_{l,k}\underline{u}_{k,t}\leq\overline{\vartheta}_{l,k,t}\\ \underline{\vartheta}_{l,k,t}\leq g_{l,k}\overline{u}_{k,t}\leq\overline{\vartheta}_{l,k,t}\\ \underline{\theta}_{l,t}\leq\sum_ig_{l,i}\overline{R}_{i,t}-\sum_jg_{l,j}\underline{S}_{j,t}\leq\overline{\theta}_{l,t}\\ \underline{\theta}_{l,t}\leq-\sum_jg_{l,j}\underline{S}_{j,t}\leq\overline{\theta}_{l,t}\\ \underline{\theta}_{l,t}\leq\sum_ig_{l,i}\underline{R}_{i,t}\leq\overline{\theta}_{l,t}\\ \underline{\theta}_{l,t}\leq\sum_ig_{l,i}\underline{R}_{i,t}-\sum_jg_{l,j}\overline{S}_{j,t}\leq\overline{\theta}_{l,t}\end{cases}\tag{60}$$

$$\underline{T}_l\leq L_{l,t}+\sum_k\underline{\vartheta}_{l,k,t}+\underline{\theta}_{l,t},L_{l,t}+\sum_k\overline{\vartheta}_{l,k,t}+\overline{\theta}_{l,t}\leq\overline{T}_l\tag{61}$$

Secondly, we ignore the non-convex constraint (52) of the natural gas system and optimize the baseline cost and the allowable upward wind power fluctuations, as shown in (61), such that the problem to obtain the initial values of the variables involved in DC constraints is convex.

$$\min_{x}\left\{\sum_{t}\sum_{i\in\Omega_{cc}}C_i(P_{i,t}^{agc})+\sum_{t}\sum_{m\in\Omega_{oc}}C_m(P_{m,t}^{nagc})+\sum_{t}\sum_{h}p_h q_{h,t}^{s}+\sum_{t}\sum_{j}p_j q_{j,t}^{p2g}+W\left(\sum_{k}(P_{k,t}^{w,e}-P_{k,t}^{w})+\bar{\pi}-\bar{\tilde{\pi}}_t\right)+W\left(\sum_{k}(P_{k,t}^{w,e}-P_{k,t}^{w})+\bar{\pi}-\bar{\tilde{\pi}}_t^{agc}\right)\right\} \tag{62}$$

C. Sequential Optimization Framework

The sign variables $\sigma_{t,w,s}$ in the objective function of the SSRO also bring challenges for solving the problem and need to be determined in advance. In order to deal with the non-convex constraints and the sign variables together, we propose a two-step sequential optimization framework for real-time dispatch, as shown in Fig. 2, and the detailed steps are described as below.

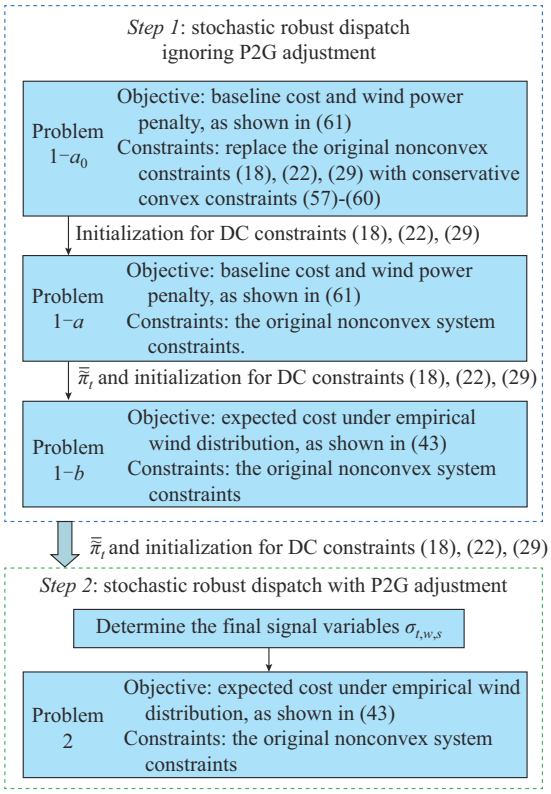

Fig. 2. Two-step sequential optimization framework for real-time dispatch.

Step 1: ignore the P2G adjustment for the wind power fluctuations and solve the stochastic robust dispatch model to obtain the sign variables $\sigma_{t,w,s}$. The process is divided into two sub-steps. In each sub-step, let $\beta_{j,t}^{-},\beta_{j,t}^{+},\underline{S}_{j,t},\overline{S}_{j,t}$ be 0.

1) Solve the traditional real-time robust dispatch without the P2G adjustment. To be specific, optimize the objective function (61) with system constraints, where nonlinear constraints (18), (22), (29) are replaced by (57)-(60) for the initial solution (denoted as Problem $1-a_0$). Then, use the results of Problem $1-a_0$ as the initial solution, and optimize the objective function (61) with the original DC constraints (18), (22), (29) (denoted as Problem $1-a$) to obtain the approximated allowable upward wind power fluctuations $\bar{\tilde{\pi}}_t$.

2) Solve the stochastic robust dispatch model without the P2G adjustment. Here, the uncertainty set is divided into two segments, i.e., $\pi_t\le 0$ and $\pi_t>0$. Compare $\bar{\tilde{\pi}}_t$ in Problem $1-a$ with the estimate points $\hat{\pi}_{t,w}$, and the sign variables of each estimate point can be obtained. Then, with the solution from Problem $1-a$ as the initial point, solve the SSRO without the P2G adjustment (denoted as Problem $1-b$).

Step 2: solve the stochastic robust dispatch model with the P2G adjustment (denoted as Problem 2). Based on the results $\boldsymbol{x}^{**}$ of Problem $1-b$, the approximated allowable wind power boundaries can be calculated by $\underline{\tilde{\pi}}_t^{p2g,*}=\max\left(\underline{\pi}_t,-\sum_j P_{j,t}^{p2g,**}\right)$, $\bar{\tilde{\pi}}_t^{agc,*}=\bar{\tilde{\pi}}_t^{**}$, $\bar{\tilde{\pi}}_t^{*}=\bar{\tilde{\pi}}_t^{**}$. Compare these boundary values with the estimate points ($\hat{\pi}_{t,w}$), and the final signal variable $\sigma_{t,w,s}$ of each estimate point can be obtained. Then, with the solution from Problem $1-b$ as the initial point, solve the SSRO with adjustment of AGC units and P2Gs for wind power fluctuations.

It should be noted that since constraint (52) only changes the gas flow distribution in the natural gas system, while has minor impacts on the power outputs of units and power input of P2Gs in the power system. Thus, the constraint (52) can be ignored in *Step 1* to accelerate the solving process. In addition, when $\bar{\tilde{\pi}}_t$ obtained in Problem $1-a_0$ is less than 0, the wind uncertainty set is divided into two segments, i.e., $\xi_{t,0}=\underline{\pi}_t,\xi_{t,1}=\bar{\tilde{\pi}}_t^{agc},\xi_{t,2}=\bar{\tilde{\pi}}_t$, and the objective function and constraints in the SSRO need to be updated accordingly.

V. Case Study: A Small-scale System

This section conducts the simulation studies on a PGIS, which combines an IEEE 39-bus system and a Belgian 20-bus natural gas system, as shown in Fig. 3. The IEEE 39-bus system contains five AGC units, three non-AGC units, and four wind farms, where two wind farms have each installed a P2G device of 60 MW. The cost and operation parameters of the coal-fired units, gas turbines, P2Gs, and gas sources are given from Tables I-IV. The natural gas system contains two gas sources. The two systems are coupled by three gas turbines and two P2Gs. The wind power is assumed to satisfy the Gaussian distribution. The dispatch time period is from 06:00 p.m. to 07:00 p.m.. To verify the effectiveness of the proposed method, we generate 5000 stochastic scenarios based on Monte Carlo simulation (MCS) to test the optimized results. The models are solved by CPLEX solver on a computer with an Intel(R) Xeon(R) Silver 4216 CPU and 16 GB RAM.

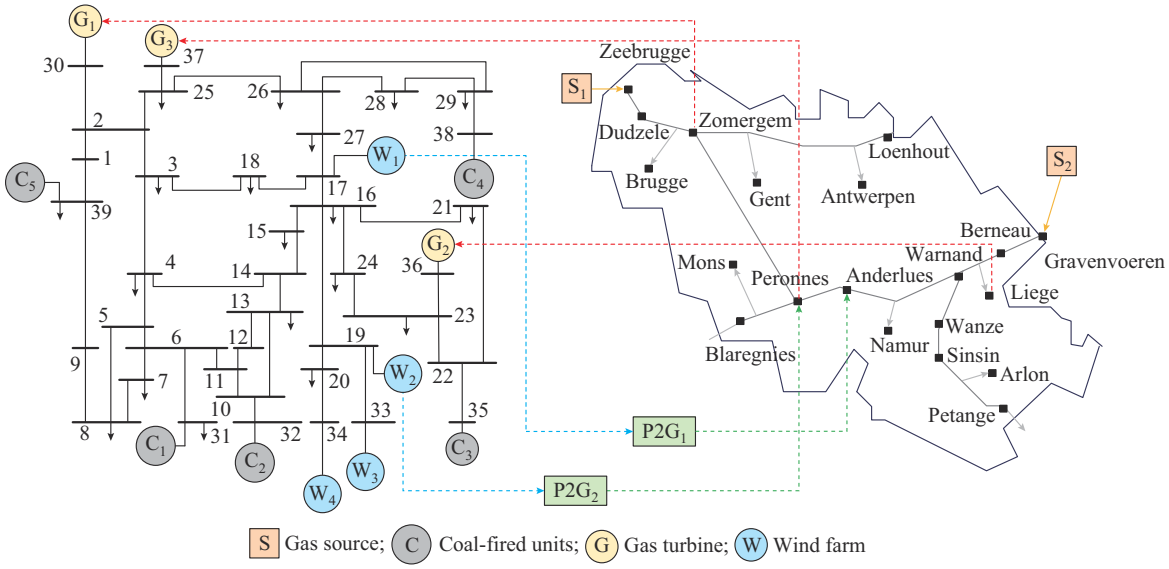

Fig. 3. Diagram of PGIS.

TABLE I
PARAMETERS OF COAL-FIRED UNITS

Unit	AGC	a ($/(MWh)^2)	b ($/MWh)	c($)	$\overline{P}$ (MW)	$\underline{P}$ (MW)	r^+/r^- (MW per 5 min)
C_1	No	0.0069	30.915	1352	455.2	135.7	45.5
C_2	Yes	0.0098	32.342	1519	507.5	152.3	50.8
C_3	No	0.0055	30.070	1353	480.9	144.3	48.1
C_4	Yes	0.0062	32.100	1984	605.5	181.7	60.6
C_5	No	0.0074	32.271	2224	770.0	231.0	77.0

TABLE II
PARAMETERS OF GAS TURBINES

Unit	AGC	η^{gt} (%)	$\overline{P}$ (MW)	$\underline{P}$ (MW)	r^+/r^- (MW per 5 min)
G_1	Yes	40	509.6	135.6	152.8
G_2	Yes	40	284.2	231.0	85.2
G_3	Yes	40	276.3	118.4	82.9

TABLE III
PARAMETERS OF P2GS

P2G	$\overline{P}^{p2g}$ (MW)	η^{p2g} (%)	p^{p2g} ($/m^3)
$P2G_1$	50	60	0.03
$P2G_2$	50	60	0.03

TABLE IV
PARAMETERS OF GAS SOURCES

Gas source	$\underline{q}^s$ (m^3/s)	$\overline{q}^s$ (m^3/s)	p^s ($/m^3)
S_1	30.79	133.29	0.3
S_2	35.90	104.23	0.3

A. Effects of P2G Participation in AGC Service

Figures 4 and 5 show the baseline power and downward/upward fluctuations (DF/UF) of wind power undertaken by the gas turbines among AGC units and the P2Gs. The results show the gas turbines operate at the lowest power due to their high generation cost.

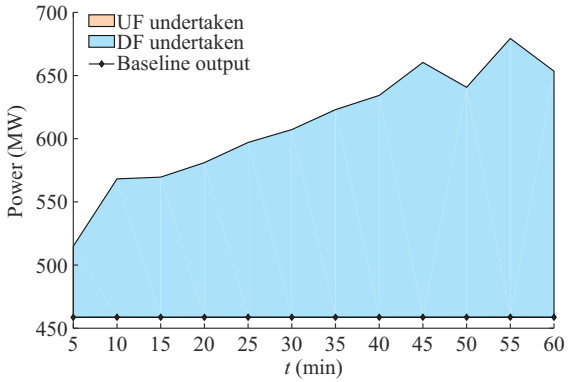

Fig. 4. Baseline power and wind power fluctuations undertaken by gas turbines among AGC units.

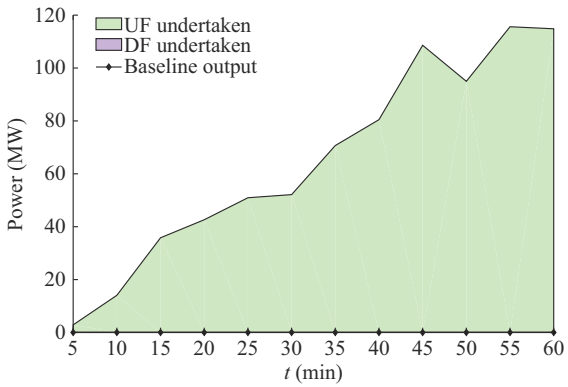

Fig. 5. Baseline power and wind power fluctuations undertaken by P2Gs.

As a result, they only undertake the DF adjustment since there is no room for a downward adjustment of the gas turbines. The baseline power of P2Gs is zero in this case because their operation costs are comparatively high, and the wind power is not redundant during this time period. Meanwhile, P2Gs undertake a large amount of UF adjustment tasks since the adjustment capability from AGC units is insufficient in this case. The results also verify the necessity to

involve the gas uncertainty issues in the security constraints of PGIS due to their highly volatile and uncertain operations caused by the wind power uncertainty.

Table V compares the optimization and MCS results with and without participation of P2G in AGC service. The results show that participation of P2G in the AGC service has overwhelming superiority in integrating uncertain wind power, and the allowable upward wind power fluctuation increases significantly from 1274.8 MW to 1918.7 MW. Meanwhile, the results show that the participation of P2G in the AGC also reduces the operation cost. The costs in MCS are close to the SSRO results, which validates the effectiveness of the multi-point estimate of the empirical distribution.

TABLE V
OPTIMIZATION AND MCS RESULTS WITH AND WITHOUT PARTICIPATION OF P2G PARTICIPATION IN AGC SERVICE

System	Optimized result		MCS result		
	$\bar{\tilde{\pi}}$ (MW)	Objective ($)	Wind curtailment cost ($)	Adjustment cost ($)	Total cost ($)
Without P2G	1274.82	229363	52.000	378	229389
With P2G	1918.70	229281	0.449	355	229309

B. Effects of Segmented Optimization

Table VI compares the optimization and MCS results of segmented and non-segmented methods. The segmented method illustrates the advantage of using fewer P2Gs. Compared with the non-segmented method in which AGC units and P2Gs respond simultaneously to the wind power fluctuations, the segmented method makes less use of the P2Gs, and their power consumption decreases largely from 71.8 MW to 14.0 MW compared with the non-segmented method. Accordingly, the adjustment cost of the segmented method is lower, which shows better economics. Meanwhile, the wind curtailment of the segmented method is less than the non-segmented method, indicating that the segmented method will not decrease wind power integration.

TABLE VI
OPTIMIZATION AND MCS RESULTS WITH NON-SEGMENTED AND SEGMENTED METHODS

Method	Optimized result ($)	MCS result			
		Wind curtailment cost ($)	P2G input (MW)	Adjustment cost ($)	Total cost ($)
Non-segmented	229399	2.22	71.82	472	229432
Segmented	229281	4.49	13.97	355	229309

Figure 6 shows the adjustment tasks undertaken by different AGC resources in SSRO. The results show that the UFs of wind power are undertaken by both the P2Gs and AGC units. Meanwhile, the AGC units undertake the UF at first, and P2Gs undertake the UF when the uncertainty is comparatively large. As for the DFs of wind power, they are all undertaken by the AGC units in this case. The reason for this result is that the baseline power of P2Gs is zero, and thus they have no more capability to undertake the adjustment task to cope with DFs of wind power.

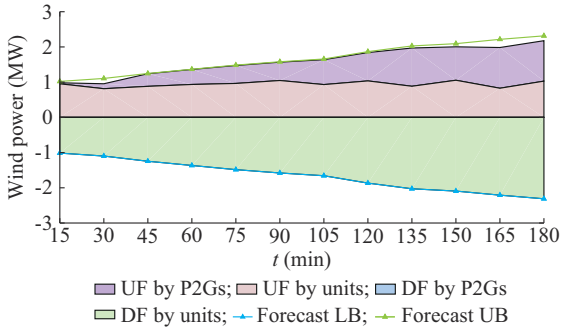

Fig. 6. Adjustment tasks undertaken by different AGC resources in SSRO.

C. Comparison of Different Robust Methods

To verify the effectiveness of the proposed SSRO method, this subsection compares SSRO with CRO [16] and DRO [41]. Note that the segmented linear decision rule is applied in all three methods for a fair comparison, thus the CRO and DRO are actually upgraded to segmented CRO and segmented DRO (SCRO and SDRO). The differences between the above methods are: SCRO optimizes the baseline cost, SDRO optimizes the expected cost of extreme distributions, and the proposed SSRO optimizes the expected cost under empirical distribution. The system security constraints of these three robust methods are the same. Table VII compares the optimization and MCS results of the three methods. The simulation is conducted with partial relaxation-based DCO. The results with original capacity of 1.00 show that SCRO is the most conservative method, which does not curtail wind power. However, integrating all the wind power is at the expense of the highest total cost in MCS. Because SCRO optimizes the baseline cost and ignores the adjustment cost, this increases the actual total cost in MCS. As for SDRO and SSRO, they optimize the expected cost and save the total cost with a small amount of wind power curtailment. Compared with SSRO, SDRO minimizes the expected cost under extreme distribution, and thus its cost is higher, especially when the actual distribution is closer to the empirical distribution rather than the extreme distribution. To test the performance when the AGC resources are insufficient, the adjustment capability, i.e., the ramping rate of the AGC units and the conversion capacity of the P2Gs, is reduced to 75% of the original data. The results show that wind curtailment is inevitable when the AGC resources are inadequate. With limited adjustment capability, the proposed SSRO can still save the total cost. Meanwhile, the computation time is the shortest with SSRO.

D. Impacts of Number of Estimate Points

In the multi-point estimate method, the number of estimate points directly affects the optimization results and the computation time. Therefore, this subsection compares the results of different numbers of estimate point. The number of the estimate points is usually selected as an odd number such as 3, 5, and 7 ($N \geq 3$).

TABLE VII
OPTIMIZATION AND MCS RESULTS OF ROBUST STRATEGIES IN ILLUSTRATIVE CASE

Capacity	Strategy	Optimization result		MCS result		
		Cost ($)	Time (s)	Wind curtailment cost ($)	Adjustment cost ($)	Total cost ($)
1.00	SCRO	230875	75	0	190	231065
	SDRO	230718	88	0.211	258	230586
	SSRO	229281	46	0.449	355	229309
0.75	SCRO	232185	161	0.680	–197	231989
	SDRO	230510	94	2.360	346	230055
	SSRO	229304	34	3.200	404	229362

Figure 7 shows that the allowable upper bound of wind power fluctuations with 3-point estimate is lower than the others. It is because the maximum CDF of 3-point estimate is 95.84%, which can hardly cover the wind power fluctuations. In contrast, the upper bounds with the 5-point and 7-point estimate are higher, while the 7-point estimate nearly reaches the forecast one since it covers 99.99% of the wind power fluctuations.

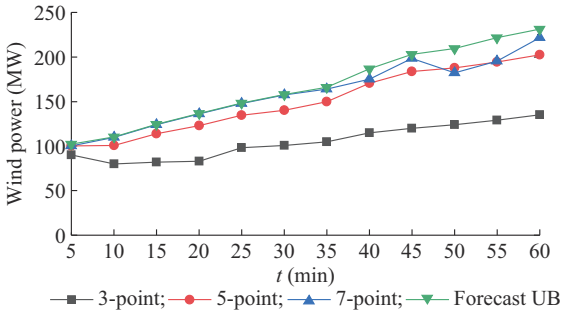

Fig. 7. Allowable upper bound of wind power fluctuation with different numbers of estimate points.

Table VIII compares the optimization results with different numbers of estimate points.

TABLE VIII
OPTIMIZATION AND MCS RESULTS WITH DIFFERENT NUMBERS OF ESTIMATE POINTS

N	Optimization result		MCS result		
	Objective ($)	Time (s)	Wind curtailment cost ($)	Adjustment cost ($)	Total cost ($)
3	229218	39	41.000	365	229359
5	229246	39	0.953	352	229307
7	229281	46	0.449	355	229309

Overall, the MCS costs of 5-point and 7-point estimate are closer to the optimized results, showing that more estimate points will lead to a more precise estimation. Note that the computation time increases along with the increase of the estimate numbers, but such an increase is acceptable. Therefore, we select 7-point estimate to formulate the expected cost objective in this paper.

E. Computation Performances

In this subsection, the partial relaxation-based DCO is compared with the original complete relaxation-based method. We also compare the results with some other methods, including the piecewise linearization method [42] and the direct NLP method [43]. The piecewise linearization method transforms the non-convex problem into MIQCP by adding integer variables, while NLP method directly uses the nonlinear solving algorithms. Table IX compares the results of the MIQCP, NLP, partial relaxation-based DCO, and complete relaxation-based DCO. The results show that the MIQCP cannot converge within the time limit, in which the added integer variables obviously slow down on the solving process.

TABLE IX
COMPARISON OF DIFFERENT OPTIMIZATION METHODS

Capacity	Method	Optimized objective ($)	Iteration	Time (s)
1.00	MIQCP	Non-convergence	Non-convergence	Non-convergence
	NLP	231261	1	319
	DCO (complete)	232791	50	213
	DCO (partial)	229281	11	31
0.75	MIQCP	Non-convergence	Non-convergence	Non-convergence
	NLP	231314	1	416
	DCO (complete)	232578	50	208
	DCO (partial)	229304	7	17

Compared with the DCOs, the optimal cost of the direct NLP is larger, and the computation time is much longer. By comparing the partial and complete relaxation-based DCO methods, it can be observed that the partial relaxation-based DCO method significantly saves computation time and iterative times. The reason is that the non-convex constraints in the power system have large influences on the objective values. When completely relaxing the non-convex constraints, the algorithm needs to search outside the feasible region for many times to enter the feasible region. To sum up, the partial relaxation-based DCO illustrates the the best performance among the four methods.

VI. CASE STUDY: A LARGE-SCALE SYSTEM

To further verify the effectiveness of the proposed model, we conduct a simulation on a large-scale PGIS, which combines the IEEE 118-bus power system [44] and a 40-bus natural gas system. The IEEE 118-bus system contains 12 AGC units, 7 non-AGC units, and 6 wind farms, where 4 wind farms have each installed a P2G device of 40 MW. The natural gas system is composed of two Belgian 20-bus natural gas systems and contains 4 gas sources. The power and gas systems are coupled by 8 gas turbines and 4 P2G devices. Table X compares the optimization and MCS results of the SSRO, SCRO, and SDRO in the large-scale system. In general, the results of the large-scale system are overall consistent with the ones of the small-scale system. In detail, SCRO only optimizes the baseline cost and integrates the

wind power as much as possible, thus leading to the highest cost. SDRO and SSRO optimize the expected cost and save the total cost with a little amount of wind curtailment. Furthermore, when the actual distribution is closer to the empirical distribution, SSRO shows better performance compared with the SDRO.

TABLE X
OPTIMIZATION AND MCS RESULTS OF DIFFERENT ROBUST STRATEGIES IN LARGE-SCALE SYSTEM

Capacity	Strategy	Optimization result		MCS result		
		Cost ($)	Time (s)	Wind curtailment cost ($)	Adjustment cost ($)	Total cost ($)
1.00	SCRO	354139	35	0	248.00	354387
	SDRO	354247	106	0.511000	–6.45	354170
	SSRO	352586	240	0.912000	191.00	352621
0.75	SCRO	354660	90	0.000134	104.00	354763
	SDRO	354364	107	0.477000	–4.66	354208
	SSRO	352701	223	11.000000	249.00	352723

VII. CONCLUSION

This paper proposes a segmented real-time dispatch model for PGIS to cooperate the traditional AGC units and P2Gs based on the segmented linear decision rule. Meanwhile, SSRO is proposed to address the wind power uncertainty in real-time dispatch, and a partial relaxation-based DCO method is developed to solve the proposed model. The participation of the P2Gs in the AGC service enhances the system capability to address the wind power uncertainty and increases wind power integration. The segmented linear decision rule assigns the adjustment task differently when wind power uncertainty falls into different segments, which reduces the total cost through better cooperation between traditional AGC units and P2Gs. Out-of-sample analysis in a testing system verifies the higher cost efficiency and better computation performance of the proposed SSRO compared to the conventional robust methods. Besides, the developed partial relaxation-based DCO illustrates faster convergence compared with other methods.

It should be noted that the proposed SSRO is based on the empirical distribution, which is a fitting distribution developed from historical data. When sufficient historical data are available and a well-done fitting method is applied, the fitted empirical distribution could probably be very close to the actual probability distribution. In such cases, SSRO will illustrate superior performance. However, SSRO can hardly guarantee good performance when the fitted empirical distribution is far away from the actual distribution. A promising way to address this problem may be to combine the empirical distribution in SSRO and the extreme distribution in SDRO to balance the economic efficiency and robustness of the real-time dispatch, which will be conducted in our future work.

REFERENCES

[1] N. Jia, C. Wang, W. Wei *et al.*, "Decentralized robust energy management of multi-area integrated electricity-gas systems," *Journal of Modern Power Systems and Clean Energy*, vol. 9, no. 6, pp. 1478-1489, Nov. 2021.

[2] H. Hui, M. Bao, Y. Ding *et al.*, "Optimal energy reserve scheduling in integrated electricity and gas systems considering reliability requirements," *Journal of Modern Power Systems and Clean Energy*, vol. 10, no. 6, pp. 1494-1506, Nov. 2022.

[3] R. Zhang, T. Jiang, F. Li *et al.*, "Conic optimal energy flow of integrated electricity and natural gas systems," *Journal of Modern Power Systems and Clean Energy*, vol. 9, no. 4, pp. 963-967, Jul. 2021.

[4] X. Zhang, K. Chan, H. Wang *et al.*, "Game-theoretic planning for integrated energy system with independent participants considering ancillary services of power-to-gas stations," *Energy*, vol. 176, pp. 249-264, Jun. 2019.

[5] J. Fang, Q. Zeng, X. Ai *et al.*, "Dynamic optimal energy flow in the integrated natural gas and electrical power systems," *IEEE Transactions on Sustainable Energy*, vol. 9, no. 1, pp. 188-198, Jan. 2018.

[6] Z. Bao, Y. Ye, and L. Wu, "Multi-timescale coordinated schedule of interdependent electricity-natural gas systems considering electricity grid steady-state and gas network dynamics," *International Journal of Electrical Power & Energy Systems*, vol. 118, p. 105763, Jun. 2020.

[7] Y. Yin, T. Liu, L. Wu *et al.*, "Day-ahead risk-constrained stochastic scheduling of multi-energy system," *Journal of Modern Power Systems and Clean Energy*, vol. 9, no. 4, pp. 720-733, Jul. 2021.

[8] Y. Li, Y. Zou, Y. Tan *et al.*, "Optimal stochastic operation of integrated low-carbon electric power, natural gas, and heat delivery system," *IEEE Transactions on Sustainable Energy*, vol. 9, no. 1, pp. 273-283, Jan. 2018.

[9] L. Bai, F. Li, H. Cui *et al.*, "Interval optimization based operating strategy for gas-electricity integrated energy systems considering demand response and wind uncertainty," *Applied Energy*, vol. 167, pp. 270-279, Apr. 2016.

[10] H. Cong, Y. He, X. Wang *et al.*, "Robust optimization for improving resilience of integrated energy systems with electricity and natural gas infrastructures," *Journal of Modern Power Systems and Clean Energy*, vol. 6, no. 5, pp. 1066-1078, Sept. 2018.

[11] C. He, T. Liu, L. Wu *et al.*, "Robust coordination of interdependent electricity and natural gas systems in day-ahead scheduling for facilitating volatile renewable generations via power-to-gas technology," *Journal of Modern Power Systems and Clean Energy*, vol. 5, no. 3, pp. 375-388, May 2017.

[12] C. He, L. Wu, T. Liu *et al.*, "Robust co-optimization scheduling of electricity and natural gas systems via ADMM," *IEEE Transactions on Sustainable Energy*, vol. 8, no. 2, pp. 658-670, Apr. 2017.

[13] W. Wei, F. Liu, and S. Mei, "Distributionally robust co-optimization of energy and reserve dispatch," *IEEE Transactions on Sustainable Energy*, vol. 7, no. 1, pp. 289-300, Jan. 2016.

[14] Z. Li, W. Wu, B. Zhang *et al.*, "Adjustable robust real-time power dispatch with large-scale wind power integration," *IEEE Transactions on Sustainable Energy*, vol. 6, no. 2, pp. 357-368, Apr. 2015.

[15] W. Zheng, X. Wang, Z. Shao *et al.*, "A modified affine arithmetic-based interval optimization for integrated energy system with multiple uncertainties," *Journal of Renewable and Sustainable Energy*, vol. 14, p. 016302, Jan. 2022.

[16] K. Qu, B. Zheng, T. Yu *et al.*, "Convex decoupled-synergetic strategies for robust multi-objective power and gas flow considering power to gas," *Energy*, vol. 168, pp. 753-771, Feb. 2019.

[17] C. Wang, W. Wei, J. Wang *et al.*, "Convex optimization based adjustable robust dispatch for integrated electric-gas systems considering gas delivery priority," *Applied Energy*, vol. 239, pp. 70-82, Apr. 2019.

[18] C. He, X. Zhang, T. Liu *et al.*, "Distributionally robust scheduling of integrated gas-electricity systems with demand response," *IEEE Transactions on Power Systems*, vol. 34, no. 5, pp. 3791-3803, Sept. 2019.

[19] A. Ratha, A. Schwele, J. Kazempour *et al.*, "Affine policies for flexibility provision by natural gas networks to power systems," *Electric Power Systems Research*, vol. 189, p. 106565, Dec. 2020.

[20] Y. Zhang, J. Le, F. Zheng *et al.*, "Two-stage distributionally robust coordinated scheduling for gas-electricity integrated energy system considering wind power uncertainty and reserve capacity configuration," *Renewable Energy*, vol. 135, pp. 122-135, May 2019.

[21] K. Qu, T. Yu, Z. Pan *et al.*, "Point estimate-based stochastic robust dispatch for electricity-gas combined system under wind uncertainty using iterative convex optimization," *Energy*, vol. 211, no. 118986, Nov. 2020.

[22] L. Ju, R. Zhao, Q. Tan *et al.*, "A multi-objective robust scheduling model and solution algorithm for a novel virtual power plant connected with power-to-gas and gas storage tank considering uncertainty and demand response," *Applied Energy*, vol. 250, pp. 1336-1355, Sept.

2019.
[23] Y. Li, F. Zhang, Y. Li *et al.*, "An improved two-stage robust optimization model for CCHP-P2G microgrid system considering multi-energy operation under wind power outputs uncertainties," *Energy*, vol. 223, p. 120048, May 2021.
[24] X. Zheng, K. Qu, J. Lv *et al.*, "Addressing the conditional and correlated wind power forecast errors in unit commitment by distributionally robust optimization," *IEEE Transactions on Sustainable Energy*, vol. 12, no. 2, pp. 944-954, Apr. 2021.
[25] W. Wang, M. Wang, X. Han *et al.*, "Distributionally robust transmission expansion planning considering uncertainty of contingency probability," *Journal of Modern Power Systems and Clean Energy*, vol. 10, no. 4, pp. 894-901, Jul. 2022.
[26] C. Wang, R. Gao, W. Wei *et al.*, "Risk-based distributionally robust optimal gas-power flow with Wasserstein distance," *IEEE Transactions on Power Systems*, vol. 34, no. 3, pp. 2190-2204, May 2019.
[27] J. Liu, Y. Chen, C. Duan *et al.*, "Distributionally robust optimal reactive power dispatch with Wasserstein distance in active distribution network," *Journal of Modern Power Systems and Clean Energy*, vol. 8, no. 3, pp. 426-436, May 2020.
[28] L. Yang, Y. Xu, J. Zhou *et al.*, "Distributionally robust frequency constrained scheduling for an integrated electricity-gas system," *IEEE Transactions on Smart Grid*, vol. 13, no. 4, pp. 2730-2743, Jul. 2022.
[29] L. Yang, Y. Xu, Z. Xu *et al.*, "Convex reformulation for two-sided distributionally robust chance constraints with inexact moment information," *Journal of Modern Power Systems and Clean Energy*, vol. 10, no. 4, pp. 1060-1065, Jul. 2022.
[30] Y. Dvorkin, H. Pandzic, M. A. Ortega-Vazquez *et al.*, "A hybrid stochastic/interval approach to transmission-constrained unit commitment," *IEEE Transactions on Power Systems*, vol. 30, no. 2, pp. 621-631, Mar. 2015.
[31] Y. Li, J. Wang, Y. Zhang *et al.*, "Day-ahead scheduling strategy for integrated heating and power system with high wind power penetration and integrated demand response: a hybrid stochastic/interval approach," *Energy*, vol. 253, p. 124189, Aug. 2022.
[32] Y. Jiang, C. Wan, C. Chen *et al.*, "A hybrid stochastic-interval operation strategy for multi-energy microgrids," *IEEE Transactions on Smart Grid*, vol. 11, no. 1, pp. 440-456, Jan. 2020.
[33] C. Zhao and Y. Guan, "Unified stochastic and robust unit commitment," *IEEE Transactions on Power Systems*, vol. 28, no. 3, pp. 3353-3361, Aug. 2013.
[34] Y. Wang, L. Tang, Y. Yang *et al.*, "A stochastic-robust coordinated optimization model for CCHP micro-grid considering multi-energy operation and power trading with electricity markets under uncertainties," *Energy*, vol. 198, p. 117273, May 2020.
[35] X. Zhang, Z. Xu, T. Yu *et al.*, "Optimal mileage based AGC dispatch of a Genco," *IEEE Transactions on Power Systems*, vol. 35, no. 4, pp. 2516-2526, Jul. 2020.
[36] K. Qu, T. Yu, S. Shi *et al.*, "Synergetic power-gas flow with space-time diffusion control of air pollutants using a convex multi-objective optimization," *IEEE Transactions on Sustainable Energy*, vol. 11, no. 2, pp. 726-735, Apr. 2020.
[37] X. Li, X. Zhang, L. Wu *et al.*, "Transmission line overload risk assessment for power systems with wind and load-power generation correlation," *IEEE Transactions on Smart Grid*, vol. 6, no. 3, pp. 1233-1242, May 2015.
[38] H. Li, Z. Lv, and X. Yuan, "Nataf transformation based point estimate method," *Science Bulletin*, vol. 53, no. 17, pp. 2586-2592, Jan. 2008.
[39] T. Lipp and S. Boyd, "Variations and extension of the convex-concave procedure," *Optimization and Engineering*, vol. 17, no. 2, pp. 263-287, Jun. 2016.
[40] Y. He, M. Yan, M. Shahidehpour *et al.*, "Decentralized optimization of multi-area electricity-natural gas flows based on cone reformulation," *IEEE Transactions on Power Systems*, vol. 33, no. 4, pp. 4531-4542, Jul. 2018.
[41] P. Xiong, P. Jirutitijaroen, and C. Singh, "A distributionally robust optimization model for unit commitment considering uncertain wind power generation," *IEEE Transactions on Power Systems*, vol. 32, no. 1, pp. 39-49, Jan. 2017.
[42] C. M. Correa-Posada and P. Sanchez-Martan. (2017, Apr.). Gas network optimization: a comparison of piecewise linear models. [Online]. Available: https://optimization-online.org/2014/10/4580/
[43] O. P. Verma, T. H. Mohammed, S. Mangal *et al.*, "Minimization of energy consumption in multi-stage evaporator system of Kraft recovery process using interior-point method," *Energy*, vol. 129, pp. 148-157, Jun. 2017.
[44] R. D. Zimmerman, C. E. Murillo-Sanchez, and R. J. Thomas, "MATPOWER: steady-state operations, planning, and analysis tools for power systems research and education," *IEEE Transactions on Power Systems*, vol. 26, no. 1, pp. 12-19, Feb. 2011.

Ying Wang received the B.S. degree in electric engineering from the Nanjing University of Aeronautics and Astronautics, Nanjing, China, in 2011, and the M.S. and Ph.D. degrees from Southeast University, Nanjing, China, in 2014 and 2018, respectively. She was a Visiting Student with Argonne National Laboratory, Lemont, USA, in 2016. She is a Lecturer at the School of Automation, Southeast University. Her research interests include power systems optimization and electricity market.

Kaiping Qu received the B.Eng. and Ph.D. degrees in power system automation from the South China University of Technology, Guangzhou, China, in 2015 and 2020, respectively. From 2019 to 2020, he was a Research Assistant at Nanyang Technological University, Singapore. He is currently a Lecturer at the School of Electrical Engineering, China University of Mining and Technology, Xuzhou, China. His research interests include robust optimization, distributed optimization of integrated energy systems, and integrated demand response.

Kaifeng Zhang received the Ph.D. degree from Southeast University, Nanjing, China, in 2004, where he joined the Faculty. His research interests include power system dispatch and control, wind power and nonlinear control, and electricity market.